Lateral torsional buckling capacity of corroded steel beams: A parametric study

Lateral torsional buckling capacity of corroded steel beams: A parametric study

G Kullashi*, S C Siriwardane and M A Atteya

Department of Mechanical and Structural Engineering and Material Science, Faculty of Science and Technology, University of Stavanger, Stavanger, Norway

* Contact Author: g.kullashi@stud.uis.no

Abstract. Thickness reduction due to uniform corrosion increases the tendency of lateral torsional buckling (LTB) of open cross-sections and it reduces the moment capacity of the beam. The effect of the various corrosion cases on the LTB moment capacity ($M_{\mathrm{b,rd}}$) of the I-beams are investigated in this paper. An analytical framework for patch corroded I-beams is introduced to provide a guideline for simulating the nonlinear lateral torsional buckling behaviour of patch corroded simple beams. Hence the effect of different corrosion scenarios to reduce the buckling reduction factor (χ_{LT}) is investigated by conducting a parametric study. Twelve different beam lengths were considered to obtain different non-dimensional slenderness ratios (λ_{LT}) in this parametric study. The degraded buckling curves were obtained for each corrosion scenarios.

1. Introduction

Outdoor structures, bridges and offshore structures are exposed to corrosion. In general, five of the most common types of corrosion affect railway bridges [1, 2]. The most common type of corrosion is general (uniform) corrosion, which occurs in a uniform pattern across the surface. In bridges, general corrosion frequently occurs where water accumulates, such as on the upper side of the bottom flange of broad flange beams, built up sections, and both flanges of built-up sections consisting of riveted angles [1, 3].

Pitting corrosion is a form of corrosion that is restricted to a small area and typically starts with a surface irregularity and is also known as local corrosion. This type of corrosion is dangerous because it has the potential to trigger localized stress concentrations. Crevice corrosion is a form of localized corrosion that occurs when different structural components are close together, resulting in narrow spaces. When two separate metals are placed in an electrolyte and electrically linked, as is possible in bolted or welded connections, galvanic corrosion occurs. Corrosion fatigue is the mechanical degradation of a material caused by the combined action of localized corrosion and cycle loading, which is the last and most common form of corrosion [4].

In general, bridge structures exposed to aggressive environmental conditions suffer from time-dependent loss of both coating and material due to corrosion. As a result, the thickness of the structural steel decreases steadily [1, 5, 6, 7, 8]. A reduction in thickness is accompanied by a reduction in a few other geometric/cross-sectional properties that govern structural behavior, such as effective cross-sectional area, moment of inertia about the y-y axis and the z-z axis, torsional constant and warping constant [1, 5, 6, 7, 8]. One of the main structural behaviors of flexural members with open cross-sections, which governs the moment capacity of the member, is the LTB and, due to patch corrosion, the buckling capacity may be reduced affecting the overall stiffness of the structure.

A lack of studies is found in literature related to the simulation of the effect of corrosion in the reduction of the lateral torsional buckling moment capacity ($M_{\mathrm{b,Rd}}$) of open cross-sections. Even though several experimental works have been performed in order to get a better understanding of the $M_{\mathrm{b,Rd}}$ of corroded structural members, there is no generalized analytical framework to calculate the remaining elastic critical moment (M_{cr}) and the $M_{\mathrm{b,Rd}}$ on structural members exposed to corrosion scenarios which do not occur throughout the entire cross-section of the member. Alternatively, the design capacity can be determined based on simulations from finite element (FE) methods. The accurate simulation of nonlinear LTB behavior is quite challenging due to the interaction effect of local buckling behavior with both geometrical and material non-linearities and numerical discrepancies at the supports. The accuracy of the results is also dependent on the capabilities of the FE software employed for the simulation.

In order to overcome the above-mentioned research gaps, the main objective of this paper is to provide an analytical framework for patch corroded I-beams. The framework will comprise the time-dependent degradation formulas for the effective second moment of areas (I_{eff}), the effective torsional constant ($I_{\mathrm{t,eff}}$) and the effective warping constant ($I_{\mathrm{w,eff}}$), which are required to determine the time-dependent degradation of the M_{cr} and the $M_{\mathrm{b,Rd}}$ capacities. The secondary objective is to investigate the degree of effect of different patch corrosion scenarios with regards to the buckling reduction factor (χ_{LT}) versus the non-dimensional lateral torsional slenderness ratio ($\bar{\lambda}_{\mathrm{LT}}$).

2. Proposed analytical approach

The purpose for the proposed analytical approach is to estimate the effect of patch corrosion on open cross-sections. In order to determine the remaining $M_{\mathrm{b,Rd}}$, the reduction in thickness, the effective cross-sectional properties and the M_{cr} must be ascertained.

2.1. Corrosion wastage rate modelling

The formula for the time-dependent growth of corrosion wastage rate is obtained by taking into account the most common form of corrosion, such as general corrosion. Equation (1), as presented in [9], suggest that a nonlinear function can be used to predict corrosion propagation as shown below.

$$C(t) = A(t - t_0)^B; t > t_0 \quad (1)$$

where $C(t)$ is the average corrosion penetration in micrometres ($10^{-3}\ mm$), t is the age in years and t_0 is the time in years since the first appearance of signs of uniform corrosion. The model parameter *A* and the model parameter *B* are taken from previous published articles [1].

2.2. Effective cross-sectional properties

The effective cross-sectional area, the second moment of area about the major axis ($I_{\mathrm{y,eff}}$), the torsional constants ($I_{\mathrm{t,eff}}$) and the warping constants ($I_{\mathrm{w,eff}}$) can be calculated by the proposed formulae presented in the previously published paper [9]. These formulae were derived by taking the reduction of plate thickness due to uniform corrosion into account. Only the effective second moment of area about *z-z* axis is derived in this paper. The distance between the new neutral axis about the z-z axis and the initial neutral axis (i.e. the neutral axis of the uncorroded cross-section) is obtained as:

$$e_z(t) = \frac{\sum_{i=1}^{n} c_i(t) l_i y_i}{A_{eff}(t)} \quad (2)$$

where y_i is the height from initial neutral axis to the centroid of the i^{th} corroded surface as shown in Figure 1, the l_i is the length of the corrosion spread over the cross-section at the i^{th} corroded surface as shown in Figure 1, the $C_i(t)$ is the average corrosion penetration at the i^{th} corroded surface and this is generally calculated using Eq. (1) and $A_{eff}(t)$ is the effective cross-sectional area of the corroded cross-section which can be calculated by the proposed formula in the previously published paper [9]. The effective second moment of area about the *z-z* axis of the corroded cross-section is calculated as:

$$I_{z,eff} = I_{0,z} + A_0 {e_{z(t)}}^2 - \sum_{i=1}^{n} \{\Delta I_{i,z} + c_i(t) l_i [y_i + e_z(t)]^2\} \quad (3)$$

where $I_{0,z}$ is the second moment of area about the *z-z* axis of the uncorroded cross-sections, $\Delta I_{i,z}$ is the second moment of the i^{th} reduced area about its own neutral axis and A_0 is the initial cross-sectional area of the uncorroded cross-section.

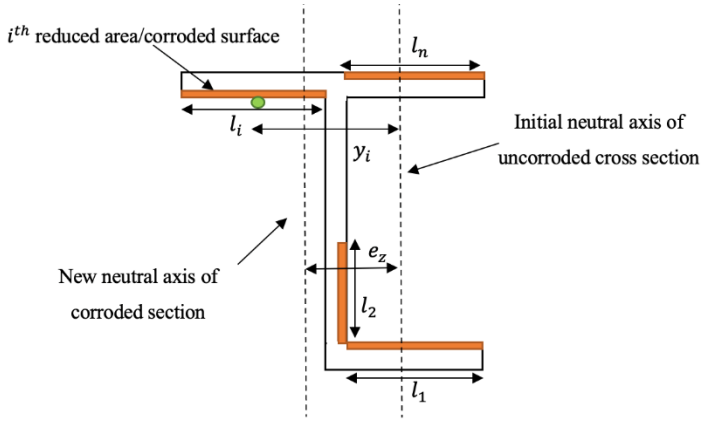

Figure 1. Schematic representations of effective cross-sectional parameters of corroded cross-sections

2.3. Elastic critical moments of corroded members

The elastic critical moment ($M_{\mathrm{cr},cor}$) is derived from the effective cross-sectional properties of the corroded beams and is presented as:

$$M_{\mathrm{cr},cor} = \sqrt{\left(\frac{\pi^2 E I_{\mathrm{z,eff}}}{L^2}\right) * \left(G I_{\mathrm{t,eff}} + \left(\frac{\pi^2 E I_{w,\mathrm{eff}}}{L^2}\right)\right)} \quad (4)$$

where E is the modulus of elasticity, $I_{\mathrm{z,eff}}$ is the corroded moment of inertia about the z-z axis, G is the shear modulus, $I_{\mathrm{t,eff}}$ is the corroded torsional constant, $I_{w,\mathrm{eff}}$ is the corroded warping constant and L is the length of the I-beam. The corroded non-dimensional slenderness $\lambda_{\mathrm{LT,cor}}$ is calculated as:

$$\lambda_{\mathrm{LT,cor}} = \sqrt{\frac{W_{\mathrm{pl,y,eff}} * f_{\mathrm{y}}}{M_{\mathrm{cr},cor}}} \quad (5)$$

where $W_{\mathrm{pl,y,eff}}$ is the corroded plastic modulus and f_{y} is the yield strength. The plastic neutral axis of the corroded cross section, y_{p} is calculated as:

$$T = C$$

$$A_{\mathrm{t}} f_{\mathrm{y}} = A_{\mathrm{c}} f_{\mathrm{y}}$$

$$y_{\mathrm{p}} = \frac{((h_{\mathrm{c}} t_{\mathrm{w}}) - (t_{\mathrm{f,c}} t_{\mathrm{w}}) - (\frac{h_{\mathrm{w}}}{2} t_{\mathrm{w}}) + (\frac{h_{\mathrm{w}}}{2} t_{\mathrm{w,c}}) + (b_{\mathrm{c}} t_{\mathrm{f,c}}) - (b t_{\mathrm{f}}) + (t_{\mathrm{f}} t_{\mathrm{w}}))}{2 t_{\mathrm{w}}} \quad (6)$$

where T is the tension force, C is the compression force, A_{t} is the tension area, A_{c} is the compression area, y_{p} is the corroded dimensional plastic neutral axis, h_{c} is the corroded height, t_{w} is the web thickness, $t_{\mathrm{f,c}}$ is the corroded flange thickness, h_{w} is the height of the web, $t_{\mathrm{w,c}}$ is the corroded thickness of the web, b_{c} is the width of the corroded part of the cross-section, b is the width of the uncorroded

part of the cross-section and t_f is the thickness of the flange. Hence, the plastic modulus $W_{pl,y,eff}$ of the corroded cross section is calculated as:

Tension part:

$$A_{t1} = bt_f$$
$$A_{t2} = (y_p - t_f)t_w$$
$$y_{t1} = y_p - t_f/2$$
$$y_{t2} = (y_p - t_f)/2$$

Compression part:

$$A_{c1} = b_c t_{f,c}$$
$$A_{c2} = h_w/2\, t_{w,c}$$
$$A_{c3} = (h_c - y_p - t_{f,c} - h_w/2)t_w$$
$$y_{c1} = h_c - y_p - t_{f,c}/2$$
$$y_{c2} = h_c - y_p - t_{f,c} - h_w/4$$
$$y_{c3} = (h_c - y_p - t_{f,c} - h_w/2)/2$$

$$W_{pl,y,eff} = A_{t1}y_{t1} + A_{t2}y_{t2} + A_{c1}y_{c1} + A_{c2}y_{c2} + A_{c3}y_{c3} \quad (7)$$

where A_{t1} and A_{t2} are the tension areas of the cross-section, y_{t1} and y_{t2} are the distances between the plastic neutral axis and the location of the application of the tension forces, A_{c1} A_{c2} and A_{c3} are the compression areas of the cross-section and y_{c1} y_{c2} and y_{c3} are the distances between the plastic neutral axis and the location of the application of the compression forces.

2.4. Corroded lateral torsional buckling moment capacity

The lateral torsional buckling moment capacity ($M_{b,Rd,cor}$) of corroded I beam is derived as,

$$M_{b,Rd,cor} = \chi_{LT,cor} W_{pl,y,eff} \frac{f_y}{\gamma_{m1}} \quad (8)$$

where, $\chi_{LT,cor} = \frac{1}{(\phi_{LT,cor} + \sqrt{\phi_{LT,cor}^2 - \lambda_{LT,cor}^2})}$

where $\phi_{LT,cor} = 0.5\left[(1 + \alpha_{LT}(\lambda_{LT,cor} - 0.2) + \lambda_{LT,cor}^2\right]$

where α_{LT} is an imperfection factor and $\chi_{LT,cor}$ is the corroded buckling reduction factor and γ_{m1} is a safety partial factor.

3. Finite element simulation

3.1. FE model

The finite element analysis (FEA) pertaining to this paper was performed using the general-purpose FE software "Ansys Workbench". The details of support/restraints are shown in Figure 2 and Table 1.

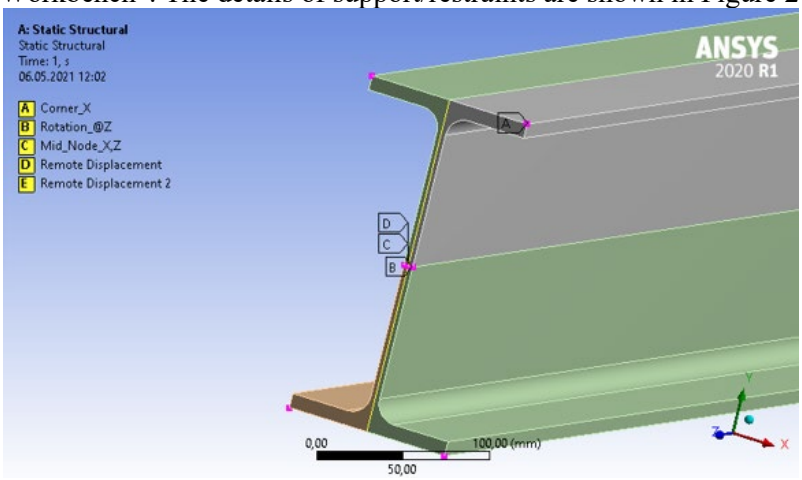

Figure 2. Boundary conditions.

Table 1. Restrained degrees of freedoms of the boundary conditions

	Ux	Uy	Uz	URx	URy	URz
Corner X (A in Fig.2)	0	0	-	-	-	-
Rotation @ Z (B in Fig.2)	-	0	-	-	-	-
Mid-node X, Z (C in Fig.2)	0	-	0	-	-	-
Remote displacement 1 (D in Fig.2)	-	0	-	-	-	-
Remote displacement 2	-	0	-	-	-	-

The Ux in the Table 1 is the displacement in the x axis, Uy is the displacement in the y axis, Uz is the displacement in the z axis, URx is the rotation about the x axis, URy is the rotation about the y axis and URz is the rotation about the z axis.

Two loading types were implemented in the FE models such as moment applied at both ends of the beam as shown in Figure 3 and uniform line pressure applied to the top flange of the beam as shown in Figure 4.

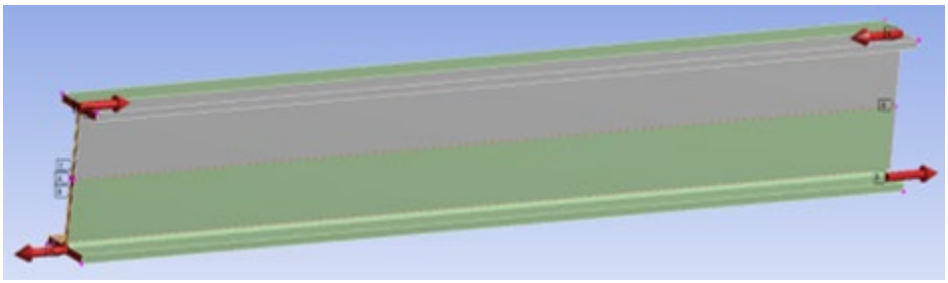

Figure 3. Moment applied at both ends of the beam.

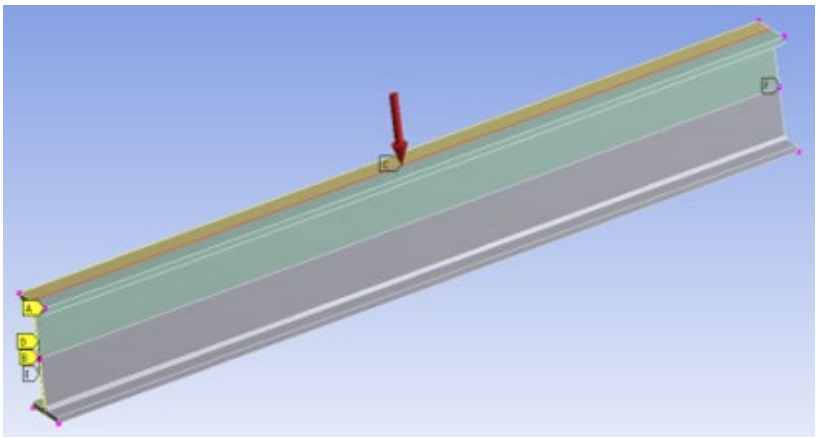

Figure 4. Uniform line pressure applied to the top flange of the beam.

In order to achieve the appropriate level of mesh convergence, both the linear and the non-linear buckling analyses were performed with various mesh densities. By decreasing the mesh density, the software uses less time to perform the analysis, but the results are less accurate. By increasing the mesh density, the software uses more time to perform the analysis and the results are more accurate. As a result, a 5 mm element size was implemented in all the FE models included in this paper. The geometrical imperfection *L/1000* was used for this study [10].

3.2. Considered corrosive cases

Three different corrosion scenarios were considered for the investigation of the LTB capacity. The beam without corrosion is investigated as a control test specimen and is designated as CNC (i.e. case no

corrosion). The case corrosion 1 (CC1) contains a corrosion case which is uniformly applied throughout the I-beam cross-section. Case corrosion 2 (CC2) contains a corrosion case which is uniformly applied throughout the bottom flange and the bottom section of the web of the I-beam cross-section. The dimensions as implemented in the FE models of the corrosion cases CNC, CC1 and CC2 are given on Table 2. Case corrosion 3-Model 1 (CC3-M1) contains corrosion at 1/3 of the length of the I-beam at the top flange, bottom flange, and web. In other words, the I-beam will be divided into three parts. The first - and third parts are without corrosion while the middle part is with corrosion. Case corrosion 3-Model 2 (CC3-M2) contains corrosion at 1/3 of the length of the beam at the bottom flange and the bottom section of the web. In other words, the beam will be divided in three parts. The first and third parts are without corrosion while the middle part is with corrosion. The dimensions of the CC3 models are given on Table 3.

Table 2. Dimensions and parameters for corrosive cases CNC, CC1 and CC2.

	CNC	CC1	CC2
Total height	200 mm	196.91 mm	198.45 mm
Top flange width	90 mm	86.91 mm	90 mm
Top flange thickness	11.30 mm	8.21 mm	11.30 mm
Bottom flange width	90 mm	86.91 mm	86.91 mm
Bottom flange thickness	11.30 mm	8.21 mm	8.21 mm
Web height	177.40 mm	184.92 mm	178.95 mm
Top web thickness	7.50 mm	4.41 mm	7.50 mm
Bottom web thickness	7.50 mm	4.41 mm	4.41 mm
Hypotenuse no-corrosion	7.07 mm	-	7.07 mm
Hypotenuse corrosion	-	3.97 mm	3.97 mm
$W_{\mathrm{pl,y}}$	250.92(10^3) mm^3	170.49(10^3) mm^3	199.93(10^3) mm^3
I_{zz}	1.38(10^6) mm^4	9.06(10^5) mm^4	1.14(10^6) mm^4
I_{yy}	2.16(10^7) mm^4	1.49(10^7) mm^4	1.77(10^7) mm^4
I_t	1.11(10^5) mm^4	3.72(10^4) mm^4	7.38(10^4) mm^4
I_w	1.22(10^{10}) mm^6	7.99(10^9) mm^6	9.64(10^9) mm^6

Table 3. Dimensions for corrosive cases CC3-M1 and CC3-M2.

Non corroded beam ends	CC3-M1 (mm)	CC3-M2 (mm)
Total height	200	200
Flange width	90	90
Flange thickness	11.30	11.30
Web height	177.40	177.40
Web thickness	7.50	7.50
Hypotenuse	7.07	7.07
Corroded middle section of beam	**CC3-M1 (mm)**	**CC3-M2 (mm)**
Total height	196.91	198.45
Top flange width	86.91	90
Top flange thickness	8.21	11.30
Bottom flange width	86.91	86.91
Bottom flange thickness	8.21	8.21
Web height	180.49	178.95
Top web thickness	4.41	7.50
Bottom web thickness	4.41	4.41
Hypotenuse	3.97	3.97

4. Comparison of results and discussion

4.1. Parametric study results

Table 4 shows the results obtained from the FEA ($M_{\mathrm{cr-A}}$) and from the Eurocode 3 [10] ($M_{\mathrm{cr-C}}$) for the linear buckling analysis considering all the corrosion cases and all the implemented beam lengths.

Table 4. Results-Elastic critical moment by linear buckling analysis

		Beam lengths (m)											
	Elastic critical moment (kNm)	0.55	1	1.5	2	2.3	2.5	3	3.4	4	5	7	10
CNC	$M_{\mathrm{cr-A}}$	-	190.4	111.5	76.3	63.7	57.4	45.7	39.1	31.9	23.8	14.6	7.6
	$M_{\mathrm{cr-C}}$	936.2	313.3	160.5	104.7	86.3	77.3	61.3	52.6	43.5	33.9	23.6	16.3
CC1	$M_{\mathrm{cr-A}}$	-	90.6	55.2	34.8	27.5	23.9	17.4	13.9	10.1	6.1	1.7	-1.5
	$M_{\mathrm{cr-C}}$	598.9	191.7	93.0	57.9	46.7	41.2	31.8	26.8	21.8	16.6	11.3	7.7
CC2	$M_{\mathrm{cr-A}}$	-	157.1	93.6	61.6	50.2	44.4	33.9	28.1	21.8	14.9	7.4	2.1
	$M_{\mathrm{cr-C}}$	749.8	248.0	124.8	80.4	66.0	59.0	46.3	39.6	32.6	25.3	17.5	12.0
CC3-M1	$M_{\mathrm{cr-A}}$	-	146.4	86.4	59.3	49.6	44.6	35.4	30.0	24.2	17.5	9.9	4.3
	$M_{\mathrm{cr-C}}$	-	-	-	-	-	-	-	-	-	-	-	-
CC3-M2	$M_{\mathrm{cr-A}}$	-	181.4	107.6	73.2	77.3	54.5	42.8	36.5	29.1	20.9	13.3	4.8
	$M_{\mathrm{cr-C}}$	-	-	-	-	-	-	-	-	-	-	-	-

Table 5 shows the results obtained from the Eurocode 3 [10] ($M_{\mathrm{brd-C}}$) and from the FEA (M_{brd2} and M_{brd3}) for the nonlinear buckling analysis considering all the corrosion cases and all the implemented beam lengths.

Table 5. Results- lateral torsional buckling moment capacity by nonlinear buckling analysis.

		Beam lengths (m)											
Torsional buckling moment (kNm)		0.55	1	1.5	2	2.3	2.5	3	3.4	4	5	7	10
CNC	$M_{\mathrm{brd-C}}$	93.5	83.9	72.0	60.5	54.5	50.9	43.5	38.9	33.5	27.2	19.8	14.2
	M_{brd2}	-	60.0	67.3	53.4	47.0	41.0	36.0	33.0	20.0	18.0	9.0	-
	M_{brd3}	-	65.3	70.7	59.5	54.0	50.6	44.3	40.0	36.0	30.0	17.0	-
CC1	$M_{\mathrm{brd-C}}$	63.3	56.1	46.3	36.7	32.0	29.4	24.1	21.0	17.6	13.9	9.8	6.9
	M_{brd2}	-	40.0	38.0	27.0	24.0	22.1	18.0	16.0	10.0	7.0	3.5	6.6
	M_{brd3}	-	46.1	45.4	35.6	31.0	28.7	24.0	21.5	18.8	13.0	7.0	6.6
CC2	$M_{\mathrm{brd-C}}$	74.5	66.8	56.9	47.3	42.3	39.4	33.4	29.7	25.4	20.5	14.8	10.6
	M_{brd2}	-	45.2	55.5	44.4	34.0	33.0	27.0	24.0	16.0	12.5	6.5	-
	M_{brd3}	-	53.1	59.5	49.1	44.0	41.2	34.4	32.4	28.0	23.0	13.5	-
CC3-M1	$M_{\mathrm{brd-C}}$	-	-	-	-	-	-	-	-	-	-	-	-
	M_{brd2}	-	53.3	50.0	43.0	38.0	36.0	31.5	28.1	22.0	20.0	12.0	-
	M_{brd3}	-	57.6	54.0	48.3	45.0	42.4	37.5	34.0	26.7	25.9	17.0	-
CC3-M2	$M_{\mathrm{brd-C}}$	-	-	-	-	-	-	-	-	-	-	-	-
	M_{brd2}	-	55.0	63.0	54.0	45.0	42.0	33.0	27.0	24.1	20.0	8.7	-
	M_{brd3}	-	64.0	68.6	58.0	52.4	48.9	43.1	32.5	29.5	25.5	16.0	-

4.2. Plots-Applied moment vs lateral deflection for the 5 corrosive cases and the 10 beam lengths
The following plots show the FEA results with regards to the 5 corrosive cases and the 10 beam lengths concerning the development on the decrease in the M_{brd} vs the increase in the lateral deflection.

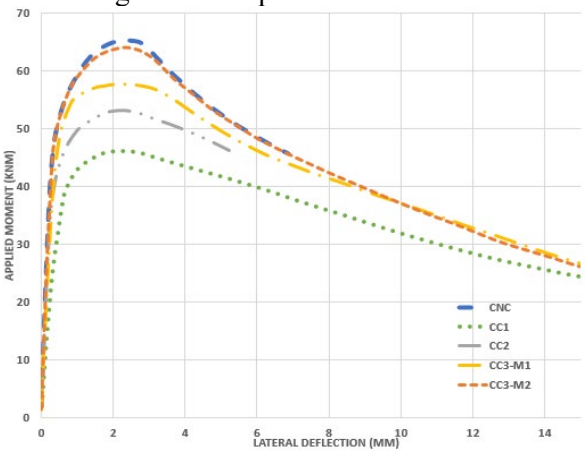

Figure 5. Applied moment vs lateral deflection, Beam length = 1 m, Imperfection = 1 mm

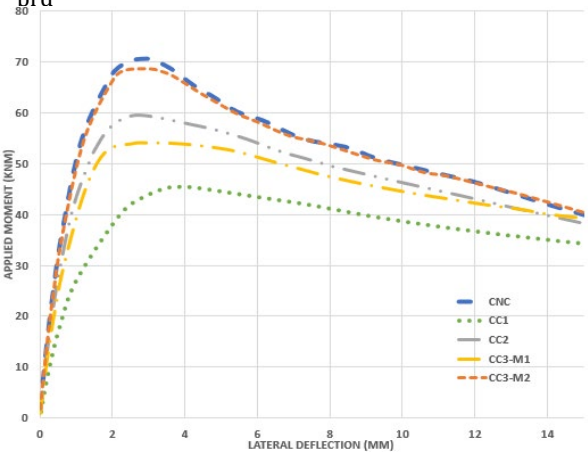

Figure 6. Applied moment vs lateral deflection, Beam length = 1.5 m, Imperfection = 1.5 mm

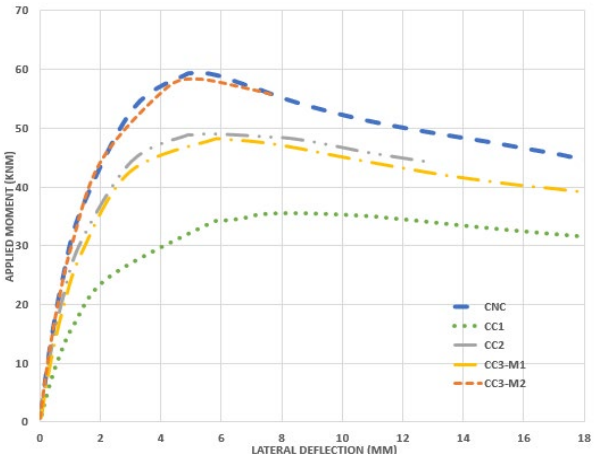

Figure 7. Applied moment vs lateral deflection, Beam length = 2 m, Imperfection = 2 mm

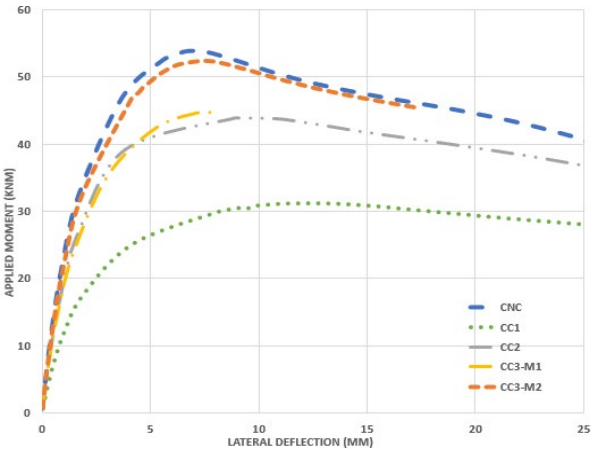

Figure 8. Applied moment vs lateral deflection, Beam length = 2.3 m, Imperfection = 2.3 mm

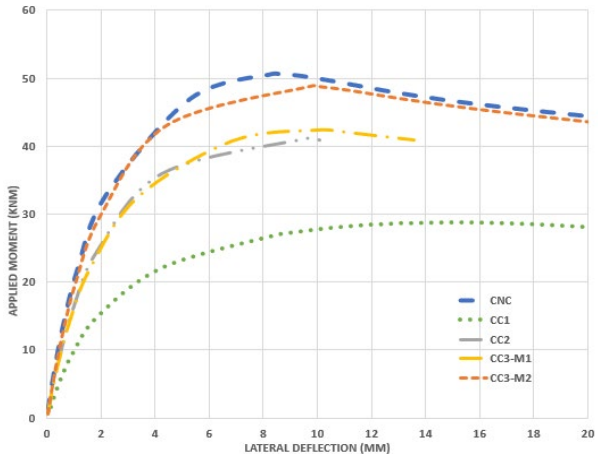

Figure 9. Applied moment vs lateral deflection, Beam length = 2.5 m, Imperfection = 2.5 mm

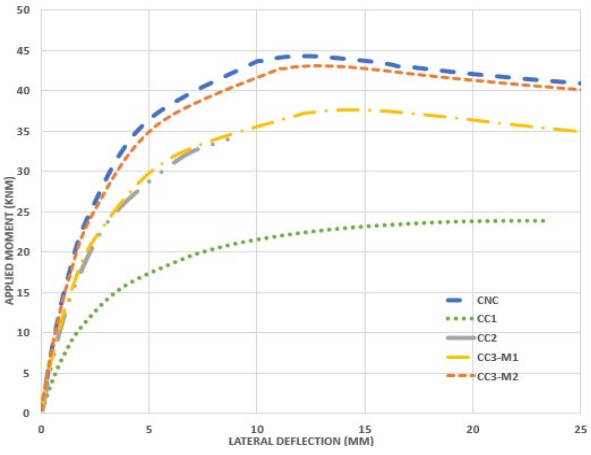

Figure 10. Applied moment vs lateral deflection, Beam length = 3 m, Imperfection = 3 mm

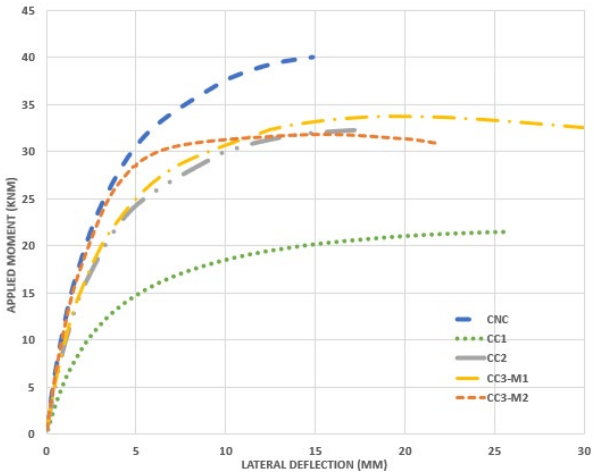

Figure 11. Applied moment vs lateral deflection, Beam length = 3.4 m, Imperfection = 3.4 mm

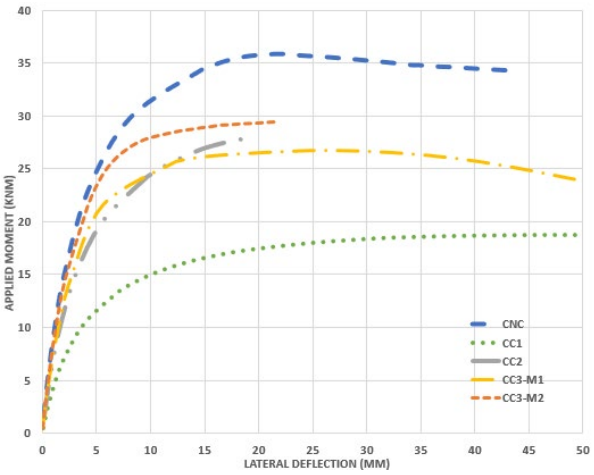

Figure 12. Applied moment vs lateral deflection, Beam length = 4 m, Imperfection = 4 mm

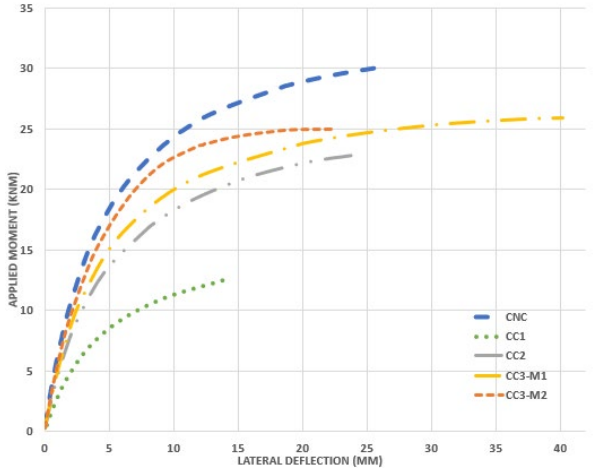

Figure 13. Applied moment vs lateral deflection, Beam length = 5 m, Imperfection = 5 mm

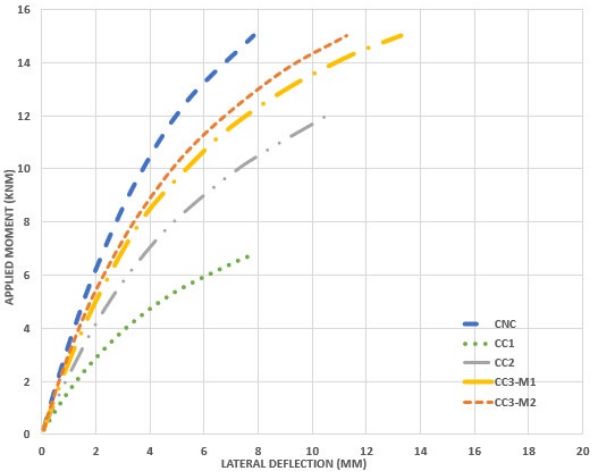

Figure 14. Applied moment vs lateral deflection, Beam length = 7 m, Imperfection = 7 mm

4.3. Plots-Lateral torsional buckling curves

The following plots show the Eurocode 3 [10] results for the CNC corrosive case and the results from the proposed analytical approach for the CC1 and CC2 corrosive cases vs the FEA results concerning the development on the λ_{LT} versus the $\mathcal{X}_{\mathrm{LT}}$ and the development on the λ_{LT} versus the M_{brd}.

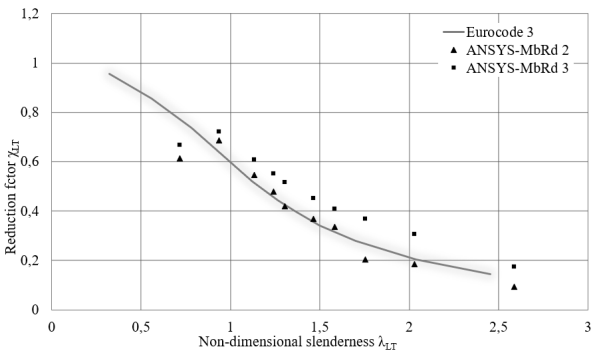

Figure 15. Reduction factor vs non-dimensional slenderness-CNC

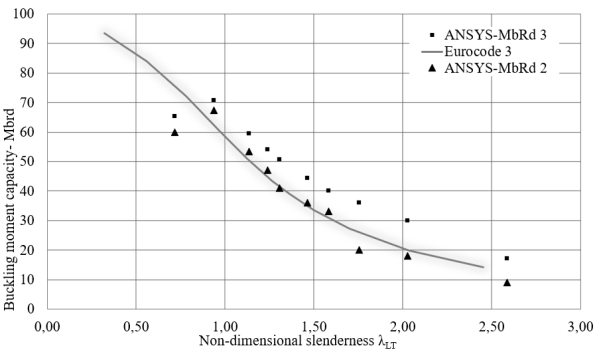

Figure 16. Buckling moment capacity vs non-dimensional slenderness-CNC

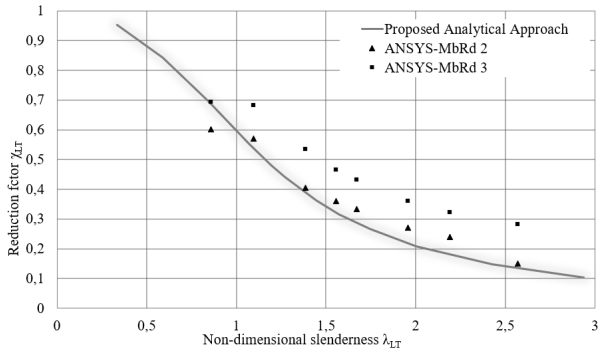

Figure 17. Reduction factor vs non-dimensional slenderness-CC1

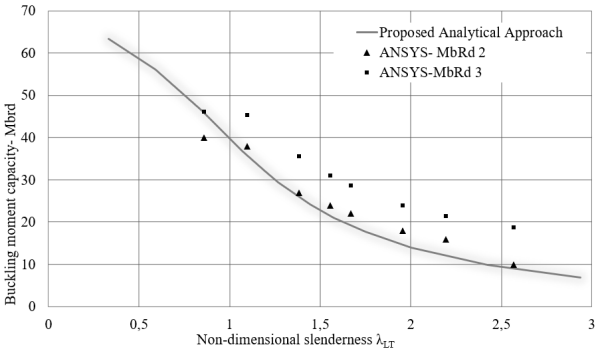

Figure 18. Buckling moment capacity vs non-dimensional slenderness-CC1

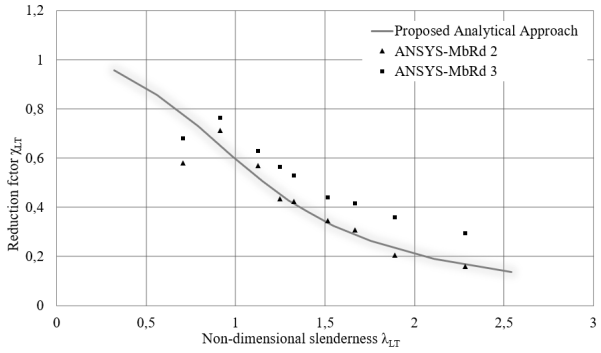

Figure 19. Reduction factor vs non-dimensional slenderness-CC2

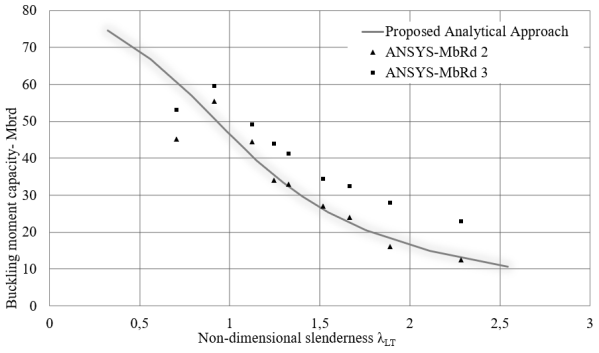

Figure 20. Buckling moment capacity vs non-dimensional slenderness-CC2

The lateral torsional buckling curves presented in Figures 15 and 16, which apply to the case no corrosion (CNC), show that the buckling capacities M_{brd2} and M_{brd3} obtained from the FEA matched with those obtained from the Eurocode 3 [10] except for the LTB non-dimensional slenderness (λ_{LT}) is equal to 0.7 where the values for M_{brd2} and M_{brd3} deviate from the value obtained from the Eurocode 3 [10].

The lateral torsional buckling curves presented in Figures 17 and 18, which apply to the case corrosion 1 (CC1), show that the buckling capacities M_{brd2} and M_{brd3} obtained from the FEA matched with those obtained from the proposed analytical approach.

The lateral torsional buckling curves presented in Figures 19 and 20, which apply to the case corrosion 2 (CC2), show that the buckling capacities M_{brd2} and M_{brd3} obtained from the FEA matched with those obtained from the proposed analytical approach, except for when the LTB non-dimensional slenderness (λ_{LT}) is equal to 0.7 where the values for M_{brd2} and M_{brd3} deviate from the value obtained from the proposed analytical approach.

5. Conclusions

The LTB moment capacity of I-beams, which were subjected to five different corrosion scenarios, were investigated in this paper using the finite element method employed ANSYS Workbench program. Only the effect of uniform corrosion was considered in this study and the following general conclusions are made based on the outcomes of this research study.

The results presented in Figure 5 to Figure 14 show that the curves for CC1 have the lowest LTB moment capacity (M_{brd}). This conclusion is valid since in this corrosion case, the I-beam is most affected to thickness reduction due to uniform corrosion. Additionally, the curves for CC3-M2 illustrate that the LTB moment capacity (M_{brd}) reduces approximately to 48.8% due to corrosion when the length of the I-beam increases to 7m. Moreover, the LTB stiffness of the curves for CC3-M2 decreases after the

lateral deflection is approximately equal to 7 mm, especially for beam lengths 3.4 m and 4 m, due to local stress concentration and its effect on the nonlinear behaviour.

The results presented in Figures 15 and 16 show that the buckling capacities M_{brd2} and M_{brd3} obtained from the FEA matched with those obtained from the Eurocode 3 [10], except for when the "non-dimensional slenderness for LTB" (λ_{LT}) is equal to 0.7 and where the values for M_{brd2} and M_{brd3} deviate from the value obtained from Eurocode 3 [10]. The reason for this discrepancy may be the interaction between local buckling and the LTB as short members are more exposed to local plate buckling.

The results presented in Figures 17 and 18 show that the buckling capacities M_{brd2} and M_{brd3} obtained from the FEA matched with those obtained from the proposed analytical approach and this confirmed the validity of the proposed analytical approach for LTB moment capacity of corroded members.

The results presented in Figures 19 and 20 show that the buckling capacities M_{brd2} and M_{brd3} obtained from the FEA matched with those obtained from the proposed analytical approach, except for when the non-dimensional slenderness for LTB (λ_{LT}) is equal to 0.7 and where the values for M_{brd2} and M_{brd3} deviate from the value obtained from the proposed analytical approach. The reason for this discrepancy may be the interaction between local buckling and the LTB as mentioned above. The discrepancy between the used non-linear material behaviour of steel and the real behaviour may also affect the deviation of the mentioned buckling capacities of the beam. Therefore, FEA of LTB behaviour of short beams is recommended for future studies. A similar study with different beam parameters and experimental comparisons of analytical LTB capacities are recommended for future studies.

References

[1] Y. Sharifi and J. K. Paik, Ultimate strength reliability analysis of corroded steel-box girder bridges*, Thin-Walled struct.,* **49***,* 157-166, 2011.

[2] J. R. Kayser, *The effects of corrosion on the reliability of steel girder bridges*, PhD thesis Ann Arbor. Mich., USA, University of Michigan, 1988.

[3] J. K. Paik, J. M. Lee and M. J. Ko, Ultimate shear strength of plate elements with pit corrosion wastage*, Thin-Walled Struct.,* 1161-1176, 2004.

[4] W. Glaser and L. G. Wright, *Mechanically assisted degradation, ASM handbooks, ASM internationals,* 137-144, 1992.

[5] Z. X. Li and T. H. T. Chan, Fatigue criteria for integrity assessment of long span steel bridge health monitoring*, Theo. App. Fract. Mech.,* **46***,* 114-127, 2006.

[6] K. Lima, N. Robson, S. Oosterhof, S. Kanji, J. DiBattista and C. J. Montgomery, Rehabilitation of a 100-year-old steel truss bridge*, CSCE 2008 Annual Conference,* 10-13, 2008.

[7] S. Nakamura and K. Suzumurab, Hydrogen embrittlement and corrosion fatigue of corroded bridge wires*, J. Constr. Steel. Res.,* **65***,* 269-267, 2009.

[8] Y. Yukikazu and K. Makoto, Maintenance of steel bridges on Honshu-Shikoku crossing*, J. Constr. Steel. Res.,* **58***,* 131-150, 2002.

[9] N. D. Adasooriya og S. C. Siriwardane, *Remaining fatigue life estimation of corroded bridge members,* Department of Structural and Mechanical Engineering and Material Science, UiS*,* 2014.

[10] NS-EN 1993-1-:2005+A1:2014+NA:2015, *Eurocode 3: Design of steel structures part 1-1: General rules and rules for buildings,* 2015.